Sustainable Cities and Society 130 (2025) 106526

Contents lists available at ScienceDirect

Sustainable Cities and Society

journal homepage: www.elsevier.com/locate/scs

How complex terrains reshape urban wind patterns and cooling effects: Evidence from a high-density weather observation network in Hangzhou Bay, China

Bu Yu [a,b,d,e], Zhiwen Luo [c,d,*], Feng Chen [g], Peng Xie [f], Shiguang Miao [b], Yige Zhong [a]

[a] Hangzhou Meteorological Bureau, Hangzhou 310051, PR China
[b] Key Laboratory of Urban Meteorology, Institute of Urban Meteorology, China Meteorological Administration, Beijing 100089, PR China
[c] School of Public Health, Zhengzhou University, Zhengzhou 450001, PR China
[d] Welsh School of Architecture, Cardiff University, UK
[e] Hangzhou International Urbanology Research Center For Urban Governance Studies, Hangzhou 311121, PR China
[f] School of Civil Engineering and Geomatics, Shandong University of Technology, Zibo 255000, PR China
[g] Zhejiang Institute of Meteorological Sciences, Hangzhou 31000, PR China

A R T I C L E I N F O

Keywords:
Urban Heat Island (UHI)
Urban climate
Cooling effect
meteorological observation
Local wind
Sea-land breeze

A B S T R A C T

Understanding how complex terrain influences urban wind patterns and cooling effects is crucial for addressing urban heat island (UHI) impacts and promoting climate-resilient cities. This study explores how terrain and urbanization jointly shape local wind systems and cooling in the Hangzhou Bay area, China, utilizing observational data from up to 574 meteorological stations (July–September, 2017–2021). Mixed local circulations occur 29–57 % of the time. In this region, strong UHI intensity can advance or delay local wind onset by 1–2 h and modify wind direction transitions, with clear west–east contrasts linked to the area's specific terrain—mountains to the west, sea to the east. These findings reflect localized interactions rather than universal patterns. Nocturnal mountain winds contribute over 2.5°C·h of cooling, especially from 17:00 to 19:00, with effects lasting ~9 h - significantly stronger than those of daytime sea breezes. However, these winds may intensify UHI effects by disproportionately cooling rural over urban areas. The results highlight the importance of region-specific station selection when assessing UHI, to avoid misinterpretations driven by local wind influences. This work provides actionable insights for improving urban ventilation and thermal comfort in complex terrain settings.

1. Introduction

Local thermal circulations, such as sea-land breezes, valley winds, and urban heat island (UHI) circulations, play a crucial role in shaping urban climate and air quality under weak synoptic conditions (Ribeiro et al., 2018). These wind systems can operate independently or interact, forming complex multi-scale circulation networks influenced by topography, land surface characteristics, and urbanization (Leo et al., 2015; Hirsch et al., 2021). For instance, Han et al. (2023) demonstrated that in a coastal ozone pollution episode in Hangzhou Bay, interactions between local winds were more critical than high temperatures. However, uncertainties remain regarding the spatiotemporal evolution of local wind systems, the dynamic coupling between different circulations, and their effects on urban thermal environments, particularly in regions where multiple systems coexist (Cheng et al., 2022; Freitas et al., 2007; Ooi et al., 2017). Existing studies predominantly rely on numerical models, which lack high-resolution observational data for validation.

Numerical models provide essential theoretical support for local wind studies, yet their simulation accuracy is constrained by planetary boundary layer (PBL) schemes, urban canopy parameterizations, and spatial resolution, often failing to capture observed wind field evolution precisely (Keeler et al., 2012). For example, He et al. (2022) tested 11 PBL schemes for a sea breeze event in Shanghai and found that most schemes only partially matched observations, generally overestimating sea breeze intensity while underestimating land temperatures. Furthermore, He et al. (2020) highlighted inherent uncertainties in the urban canopy parameterization of the Weather Research and

* Corresponding author at: Welsh School of Architecture, Cardiff University, UK.
E-mail address: LuoZ18@cardiff.ac.uk (Z. Luo).

https://doi.org/10.1016/j.scs.2025.106526
Received 13 January 2025; Received in revised form 4 June 2025; Accepted 6 June 2025
Available online 7 June 2025

Table 1
Characteristics of the four subgroups of 49 climatic stations. Locations are shown in Fig. 1.

Categories	Number	Identification	Site Distribution / Environmental Parameters	Observation purposes
VAL-S	5	K1412, K1411, 58448, K1044, K1237	Located on open and uniform slopes /LCZ [a] B-E	Analysis of Pure Valley Wind Characteristics
SEA-S	3	K5519, K2543, K1014	Located within 5 km of the coastline /LCZ 9 & LCZ B-E	Analysis of Pure Sea Breeze Characteristics
URB-S	5	K1154, K1165, K1163, K1175, K1029	Located in the urban core / Sky view factor [b]: 0.5–0.7; Impervious surface fraction [c]: 30–50 %; LCZ 1–5	UHI Intensity Calculation
RUR-S	6	K1405, K1162, K1210, K1408, K5521, K1014	Located in the rural areas outside city /Sky view factor: 0.8–1.0; Impervious surface fraction: 0–10 %; LCZ 9 & LCZ B–E	
Other CS	30	Station numbers omitted	Mean station spacing: 6–8 km (suburban), 3–5 km (urban)	Analysis of Local Wind Interactions and Their Impact on UHI

[a] Local climate zones (LCZs) correspond to urban climate zones in Stewart and Oke (2012), which include compact high-rise (LCZ1), compact mid-rise (LCZ2), compact low-rise (LCZ3), open high-rise (LCZ4), open mid-rise (LCZ5), open low-rise (LCZ6), lightweight low-rise (LCZ7), large low-rise (LCZ8), sparsely built (LCZ9), heavy industry (LCZ10), dense trees (LCZ A), scattered trees (LCZ B), bush scrub (LCZ C), low plants (LCZ D), bare soil or sand (LCZ E), bare rock or paved (LCZ F), and water (LCZ G).
[b] Ratio of the amount of sky hemisphere visible from ground level to that of an unobstructed hemisphere.
[c] Ratio of impervious plan area (paved, rock) to total plan area (%).
[d] Except for VAL-S, the elevation of the remaining 45 CS stations is within 50 meters.

Forecasting (WRF) model, affecting its depiction of urban wind fields. To address these limitations, this study leverages a high-density meteorological observation network to analyze the spatiotemporal characteristics of various local wind systems and their interactions. This approach not only provides a more accurate representation of real-world local wind variability but also offers essential validation data for improving numerical models.

Accurately identifying local wind systems is a prerequisite for studying their interactions. However, existing observational studies primarily focus on individual wind systems, such as sea breezes defined by land-sea temperature contrasts and wind direction stability (Azorin-Molina and Chen, 2009; Prtenjak and Grisogono, 2007), or valley winds classified based on terrain slopes and wind direction relationships (Yu et al., 2021). In regions with multiple interacting wind systems, traditional methods struggle to distinguish individual contributions, leading to substantial uncertainties in local wind classification and spatial delineation (Zardi and Whiteman, 2013). To overcome this challenge, we propose a unified identification method based on a common diurnal wind characteristic—twice-daily wind direction reversals. Unlike conventional approaches that rely on specific thermal or topographic indicators, this method provides a standardized framework applicable across diverse environments, eliminating inconsistencies arising from region-specific classification criteria.

Table 2
Basic characteristics of local winds observed at meteorological stations representing four distinct local wind types.

Types	ID of station	Frequency	O_{time} (LT)	O_{wd} (°)	O_{ws} (m/s)	C_{time} (LT)	C_{wd} (°)	C_{ws} (m/s)
VAL-S	K1412	239	9.1	231	2.1	18.1	160	1.8
	K1411	233	8.8	191	1.7	18.9	66	0.9
	58448	260	9.5	71	2.6	18.3	227	1.7
	K1044	206	9.1	47	1.9	18.6	190	1.1
	K1237	269	8.8	298	1.8	17.7	144	1.1
URB-S	K1154	125	10.3	152	0.9	20.1	204	0.6
	K1165	132	10.0	105	0.7	21.7	168	0.9
	K1163	170	10.5	142	1.0	21.9	232	0.8
	K1175	176	10.2	111	1.3	21.2	209	0.7
	K1029	192	9.8	84	1.1	20.9	254	0.8
RUR-S	K1405	200	9.2	86	1.4	19.2	264	1.3
	K1162	232	8.7	118	1.3	18.3	225	1.1
	K1210	183	9.9	86	1.7	19.8	292	0.9
	K1408	137	10.1	155	1.2	20.4	227	1.0
	K5521	161	9.5	71	1.4	21.0	229	0.9
	K1014	206	9.3	102	1.9	20.5	236	2.1
SEA-S	K5519	200	8.9	123	2.7	20.1	306	2.9
	K2543	212	9.0	325	2.3	19.6	172	2.6
	K1014	—	—	—	—	—	—	—

* $\mathbf{O_{time}}$ and $\mathbf{C_{time}}$ represent the onset times of daytime and nighttime local winds, respectively, $\mathbf{O_{wd}}$ and $\mathbf{C_{wd}}$ indicate the dominant wind directions during daytime and nighttime, while $\mathbf{O_{ws}}$ and $\mathbf{C_{ws}}$ denote the average wind speeds during these periods. **Frequency** refers to the occurrence frequency of local winds at each station. The dashes in the table appear because station K1014 is classified as both a rural and a sea station.

Local wind mechanisms, such as sea breezes and ventilation corridors, play a crucial role in urban ventilation and thermal regulation (Kwok et al., 2022). However, quantifying their cooling potential and incorporating them into urban planning remains an unresolved challenge (Ng et al., 2015; Zheng et al., 2024). Traditional cooling effect assessments primarily rely on instantaneous temperature drops or remote sensing analysis of land surface temperature distributions (Falasca et al., 2024; Zhou et al., 2025). Yet, short-term temperature fluctuations caused by transient weather phenomena such as cloud cover and precipitation introduce uncertainties in cooling effect evaluations (Dai et al., 1999; Gray et al., 2010). To address this issue, we propose a standardized and generalizable metric for cooling effect assessment. This method quantifies cumulative cooling effects while filtering out confounding signals from synoptic circulations and transient weather conditions, thereby enhancing the accuracy of local wind cooling effect evaluations.

While local winds effectively reduce urban temperatures, their impact on UHI intensity—defined as the temperature difference between urban and rural areas—exhibits significant spatial heterogeneity (Morris et al., 2001). For example, Ribeiro et al. (2018) found that in São Paulo, the cooling effect of sea breezes intensified the thermal gradient between the southern plateau and the city center. Conversely, Shang et al. (2024) demonstrated that in Tianjin, sea breezes gradually reduced the urban-rural temperature difference (URTD) with changing wind directions, highlighting the critical role of local winds in modulating coastal city UHIs. However, current UHI assessments often rely on fixed reference stations, which may themselves be influenced by local wind cooling effects, leading to biased UHI intensity calculations (Kwok et al., 2022; Merlone et al., 2024; Zhou et al., 2023). Additionally, inconsistencies in reference station selection criteria among different studies further complicate intercity UHI comparisons (Liu et al., 2022; Zhou et al., 2020). This study systematically evaluates the influence of local winds on UHI reference station selection and proposes an optimized UHI assessment method to improve comparability across cities.

This study investigates multi-scale interactions of thermally driven circulations in Hangzhou Bay, China - a unique region where complex

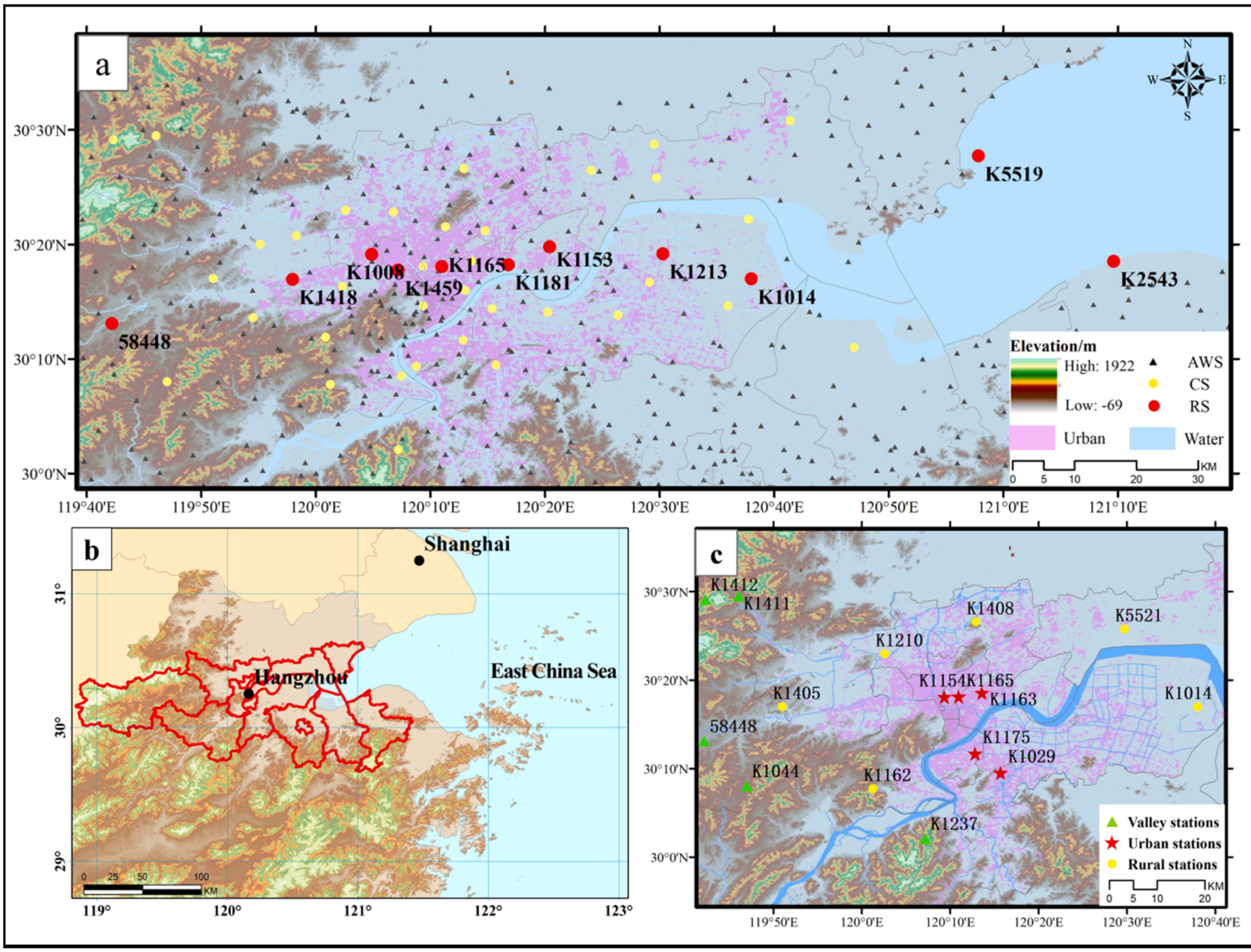

Fig. 1. (a) Map of the study area showing terrain and the locations of 574 regional meteorological stations (AWS, black triangles), including 49 climatic stations (CS, yellow circles) and 11 representative stations (RS, red circles). The station IDs for the RS are labeled in black text. (b) Surrounding topography and geographical features of the study area (outlined in red). (c) Enlarged view of the urban area within the study region, where the purple shading indicates urban boundaries. From the 49 CS, 5 urban stations (URB-S, red stars) and 6 rural stations (RUR-S, yellow circles) were selected, along with 5 valley stations (VAL-S, green triangles) and 3 sea stations (SEA-S, shown in panel a, with station IDs K5519, K2543, K1014).

topography (mountains to the west, coastal plains to the east) and rapid urbanization create dynamic interplay between mountain-valley winds, sea-land breezes, and urban heat island (UHI) effects. We employ an unprecedented high-density meteorological network (574 stations) to: (i) establish a novel framework for detecting mixed circulation regimes, (ii) quantify synergistic interactions through diurnal phase analysis, and (iii) evaluate the net thermal regulation capacity of these coupled systems and refine reference station selection criteria for UHI assessments. Our approach resolves critical gaps in understanding how mesoscale circulations modulate UHI intensity through competing warming and cooling mechanisms.

2. Study area

Hangzhou (30°16N, 120°12E), located in northern Zhejiang Province on the Hangjiahu Plain in eastern China, is a major urban center with a population of 10 million and a total area of 4,875 km^2. The region is characterized by diverse topography, with mountains to the west, south, and northwest rising to elevations of up to 1,900 meters, and the funnel-shaped Hangzhou Bay to the northeast. This west-high, east-low terrain, features a sharp elevation drop over 230 km along the WSW–ENE axis, facilitating energy and atmospheric exchanges among the ocean, mountains, and urban areas. These unique geographic conditions create an ideal setting for studying local circulation interactions.

3. Data and methods

3.1. Observation network

This study utilized meteorological data from 574 regional stations in the Hangzhou area, with a spatial resolution of approximately 3 km × 3 km. Each station recorded key variables, including air temperature, wind direction, and wind speed, at 5-minute intervals at the height of 1.5 m. Data were sourced from the National Meteorological Information Center of China and the Zhejiang Meteorological Service and underwent strict quality control protocols (Lussana et al., 2010; Wang et al., 2007). Validation steps included internal consistency checks, temporal consistency analysis, and spatial verification. Observations were excluded if daily records were incomplete ($<$22 h), wind directions remained invariant for over 3 h, or extreme values (e.g., wind speeds $>$51 m/s, temperatures $>$50°C or $<-$20°C) appeared without verification. The 574 stations primarily served two purposes: (1) analyzing typical weather cases and (2) screening representative stations for detailed local wind studies.

To align with the study's objectives, 49 climatic stations (CS) were

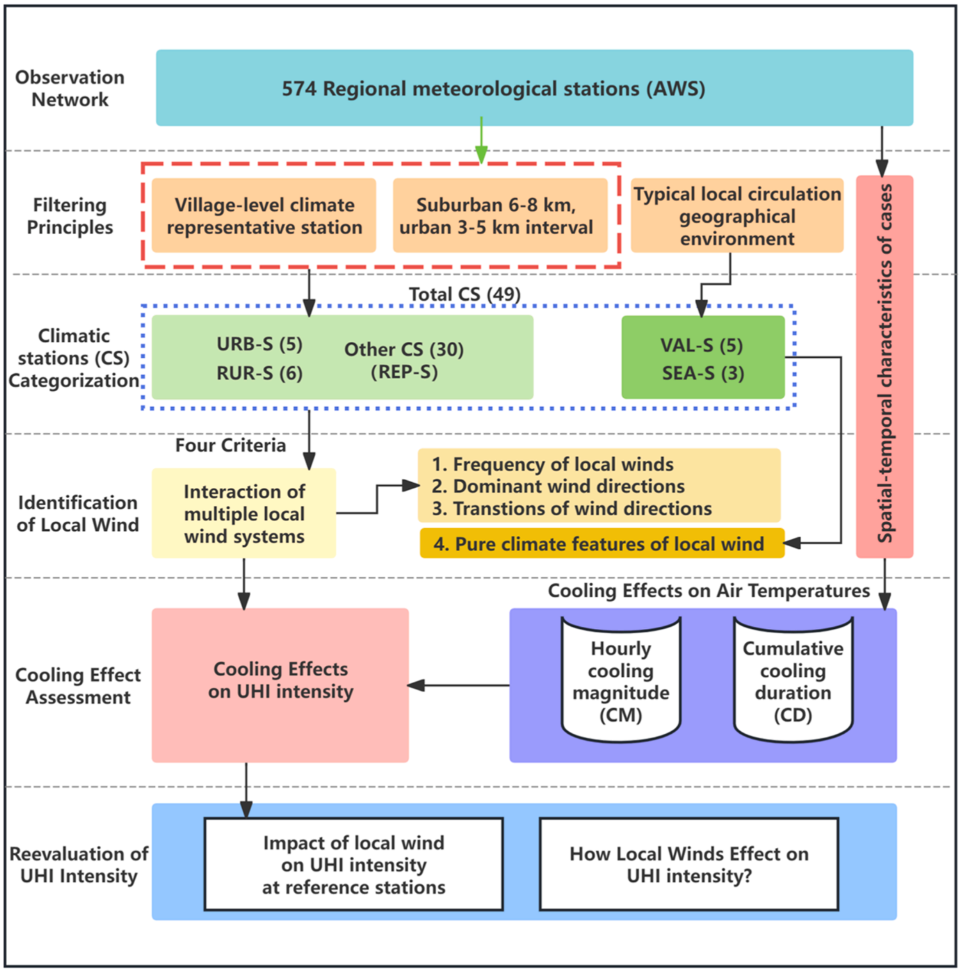

Fig. 2. Flowchart illustrating the study structure, data selection, research content, and methodology.

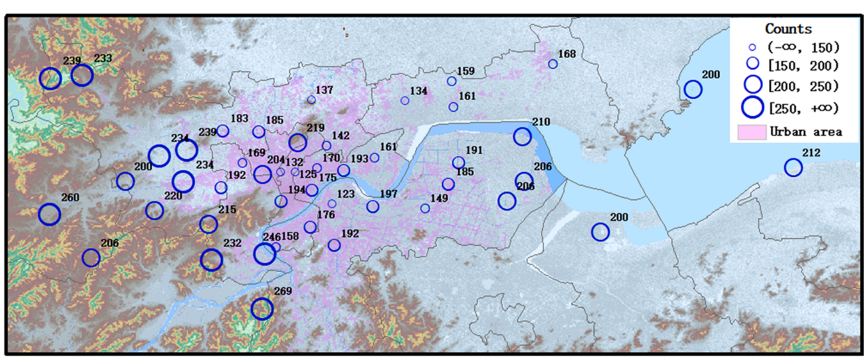

Fig. 3. Spatial distribution of cumulative local wind frequency for the 49 climatic stations (CS). Blue hollow circles represent the locations of CS stations, with larger circles indicating higher local wind frequencies. Numbers denote the counts of local wind.

selected from the 574 regional stations based on uniform observation periods (July to September, 2017-2021), data completeness, and long-term stability (>20 years). As Village-level climatic reference stations, they provide comprehensive meteorological data (wind direction, wind speed, temperature, humidity, pressure, and precipitation) and were established for regional climate monitoring. The selection process prioritized spatial consistency, excluding stations with significant wind frequency deviation (>50 % between adjacent stations) or dominant wind direction discrepancies (135°-225°without a clear transition zone). The final 49 CS were optimally distributed with an average spacing of 6-8 km in suburban areas and 3-5 km in urban areas, ensuring adequate coverage of mesoscale circulations such as mountain winds and sea breezes. Additionally, 11 representative stations (RS) along the WSW-ENE axis, spaced 20 km apart, were selected to analyze wind penetration and local circulation interactions.

The 49 CS were categorized into five subgroups based on geography and land use (Table 1): 5 valley stations (VAL-S), 3 sea stations (SEA-S), 5 urban stations (URB-S), 6 rural stations (RUR-S), and 30 other CS. VAL-S and SEA-S represent typical mountain-valley and sea-land breeze characteristics, as they are located in relatively uniform underlying surfaces with minimal external wind interference. URB-S and RUR-S were used not only for calculating urban heat island intensity but also,

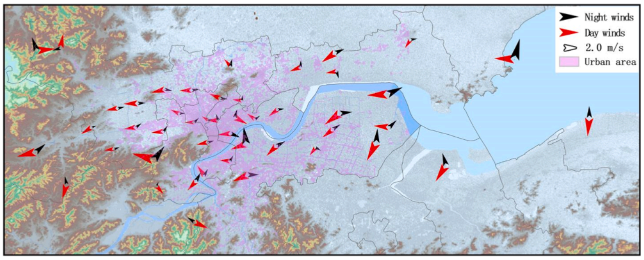

Fig. 4. Spatial distribution of dominant diurnal and nocturnal wind directions for the 49 climatic stations (CS) during local wind events. Black arrows represent the dominant nocturnal wind directions, and red arrows represent the dominant daytime wind directions, with larger arrows indicating higher wind speeds. The black hollow arrow denotes a reference wind speed of 2 m/s.

along with the remaining 30 CS, for analyzing local wind interactions in complex terrain. Selection criteria included elevation, urban morphology parameters (Sky View Factor, Impervious Surface Fraction), and the Local Climate Zones (LCZ) index, based on data from the World Urban Database and Access Portal Tools (https://www.wudapt.org/lcz/). This classification allowed for comparative analysis of pure local winds in different environments, interactions under mixed circulation conditions, and urban heat island effects (Fig. 2).

3.2. Criteria for Identifying Local Winds

The key criteria for identifying local winds are as follows:

(I). Wind Directions. Local winds exhibit peak development during 12:00-15:00 LT (daytime) and 00:00-03:00 LT (nighttime) (Junnaedhi et al., 2023). The prevailing wind directions during these periods are defined as $\mathbf{WD_d}$(daytime) and $\mathbf{WD_n}$(nighttime) directions. Wind direction must remain stable for at least 2 h within these intervals, with hourly deviations not exceeding 45°. The angular difference between $\mathbf{WD_d}$ and $\mathbf{WD_n}$ must fall within 112.5° -247.5°, ensuring consistent diurnal wind reversal. These thresholds are adapted from Yu et al. (2021), who defined similar criteria for identifying mountain winds in complex terrain.

(II). Wind Persistence. Wind direction must align with $\mathbf{WD_d}$ during the day and $\mathbf{WD_n}$ at night for at least 3 consecutive h, with a directional deviation of less than 45°.

(III). Geostrophicwind. To avoid misidentification caused by transient strong synoptic systems producing a twice-daily reversal of wind direction, only cases with 850-hPa wind speeds ($\boldsymbol{WS}_{850}$) below 10

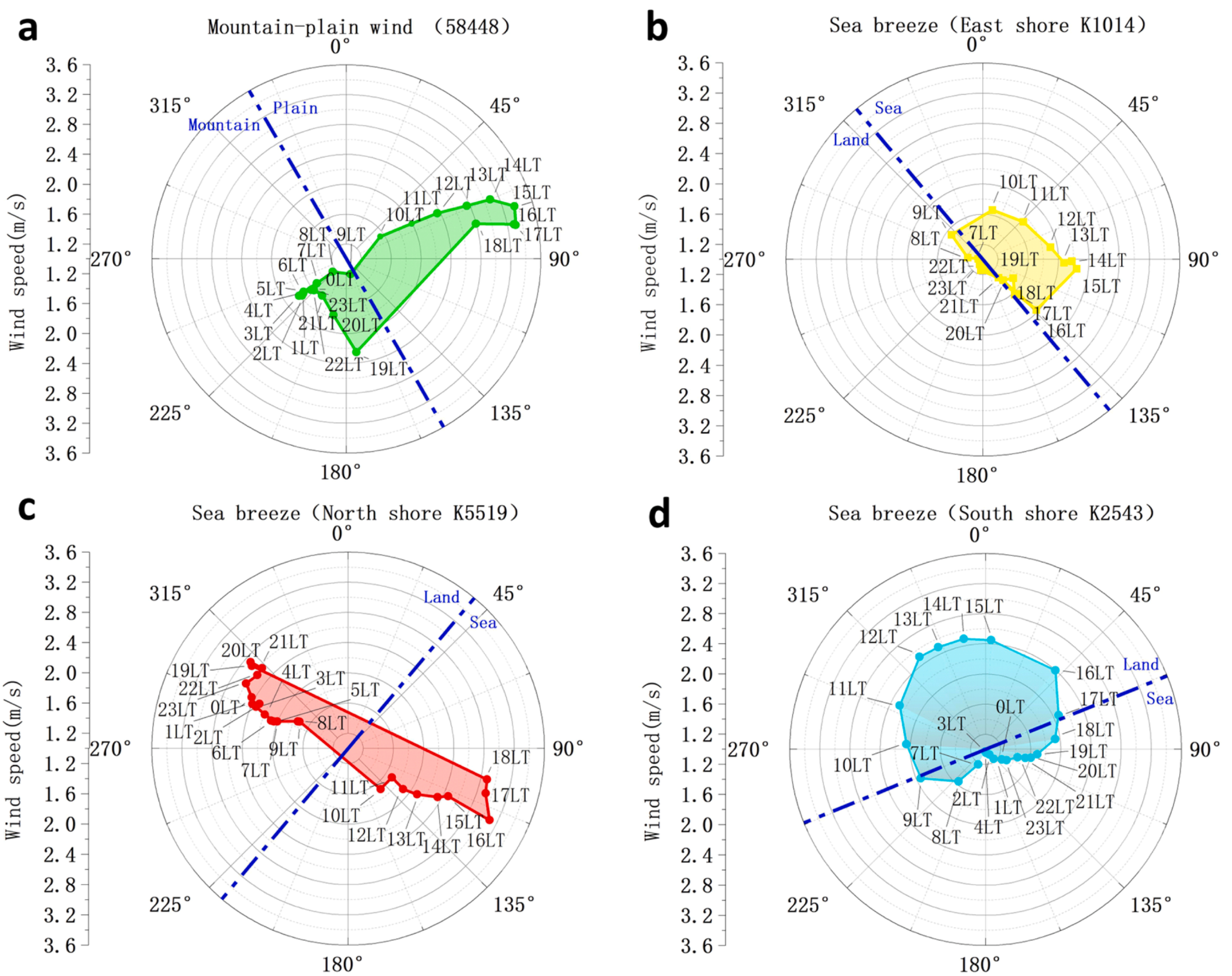

Fig. 5. Hourly wind direction variations at representative stations for mountain and sea-land breezes. (a) Mountain wind station near a plain area (ID 58448). (b) Sea-land breeze station on the western shore of Hangzhou Bay (ID K1014). (c) Sea-land breeze station on the northwestern shore of Hangzhou Bay (ID K5519). (d) Sea-land breeze station on the southern shore of Hangzhou Bay (ID K2543). Locations of these four stations are indicated in Fig. 1a.

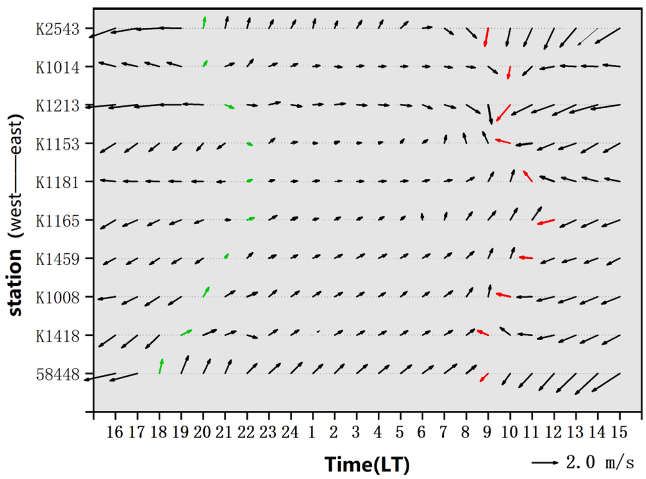

Fig. 6. Diurnal wind direction and transition patterns across 10 RS stations along the west-east transect of the study area. Black arrows indicate mean wind directions, while red arrows denote the initial wind direction at the time of transition. The reference wind speed is 2.0 m/s.

m/s are included (Arrillaga at al., 2020; Azorin-Molina at al., 2009; Junnaedhi, 2023).

(IV). Spatial Consistency. A local wind episode is confirmed when at least 50 % (more than 40) of the representative stations meet the above criteria, ensuring regional consistency (Leckebusch at al., 2006).

3.3. Calculation of cooling effect

In this study, cooling effects is calculated as the temperature difference between observed values on local wind days and the climatological mean under comparable weather conditions. The climatological mean is derived from the multi-year hourly average of the 10 days preceding and following each local wind day, provided these days meet specific criteria: cloud cover ≤8 oktas, no precipitation (< 0.1 mm), and visibility >10 km. The cooling effect of local winds is quantified using two metrics:

Cooling Magnitude (CM): Defined as the cumulative sum of deviations (°C) between the observed temperature curve during local wind events and the climatological reference curve over a specified period (Ribeiro et al., 2018). This metric is also referred to as cooling degree h (CDH) in some studies (McGarity et al., 1984). A negative sum of deviations indicates the presence of cooling effect, whereas a positive value suggests no cooling effect.

Cooling Duration (CD): Defined as the total time (hours) during which negative temperature deviations occur within the same period.

$$CM = \sum_{t \in T} [T_{OBS}(\Delta t) - T_{CLIM}(\Delta t)] \tag{1}$$

$$T_{OBS}(\Delta t) = \sum_{t=2}^{n} T_{OBS(t)} - T_{OBS(t-1)} \tag{2}$$

$$T_{CLIM}(\Delta t) = \sum_{t=2}^{n} T_{CLIM(t)} - T_{CLIM(t-1)} \tag{3}$$

$$T = \{t : \ T_{OBS}(\Delta t) < T_{CLIM}(\Delta t)\} \tag{4}$$

$$CD = \sum_{t \in T} \Delta t \tag{5}$$

Where $T_{OBS(t)}$ is the observed temperature at hour t, and $T_{OBS(t-1)}$ is the temperature at the previous hour. $T_{CLIM(t)}$ is the multi-year hourly average temperature for hour t, calculated over the 10 days before and after the local wind day under similar weather conditions. To ensure robustness, the weather conditions must also satisfy the third criterion of the 'Key Criteria for Identifying Local Winds' specifically the geostrophic wind threshold. Furthermore, any day with precipitation greater than 0.1 mm is excluded, thereby removing the influence of strong winds and rainfall events that may cause abnormal temperature fluctuations. Additionally, T represents all time intervals during which the observed hourly temperature variation $T_{OBS}(\Delta t)$ is less than the climatological reference hourly temperature variation $T_{CLIM}(\Delta t)$, Δt denotes the duration of each time step (e.g., 1 hour for hourly data), calculated as follows Eq. (1-5).

3.4. Identification of UHI

Following the regulation and index system for urban climate zones of Stewart and Oke (2012), 5 URB-S and 6 RUR-S were selected. The UHI intensity was calculated using the mean temperatures of the selected URB-S (T_{URB}) and RUR-S (T_{RUR}), and expressed as ($\Delta T_{UHI} = T_{URB} - T_{RUR}$).

To analyze the interactions among multiple local circulations, a set of filters was applied to identify 86 strong and 67 weak UHI intensity cases from the observed valley wind episodes (Dupuis et al., 2020). For classification, weak UHI cases were defined by a daily average $\Delta T_{UHI} < 0.5$°C and a maximum daily $\Delta T_{UHI} < 1.5$°C, while strong UHI cases required $\Delta T_{UHI} > 1.5$°C on average and a maximum $\Delta T_{UHI} > 3.0$°C. In both cases, the defined UHI intensity thresholds had to persist for more than 5 h.

4. Results and discussion

4.1. Spatial distribution and climatic features of local wind systems

From July to September during 2017–2021, local circulation episodes occurred 134–260 times annually, with frequencies ranging from 29 % to 57 % (Fig. 3). Higher frequencies were concentrated near the Hangzhou Bay coastline and mountainous areas, exceeding 200 episodes, while urban areas recorded fewer (~150 episodes). This distribution likely reflects the influence of mountain winds from the west and sea-land breezes from the east, with urban roughness and UHI circulation limiting the extent of local winds (Barlow et al., 2014). Mountainous areas showed slightly higher frequencies than coastal regions, likely due to Hangzhou Bay's narrow inlet restricting sea breeze penetration inland (Alomar-Garau et al., 2022). The broader spatial influence of mountain winds further highlights their stronger impact compared to sea-land breezes, consistent with the findings of Yu et al. (2021).

Regarding wind direction, Valley and Coastal stations showed clear geographical influences, characterized by terrain-dependent wind patterns, while most other stations experienced easterly winds during the day and westerly winds at night (Fig. 4). These patterns align with theoretical expectations: easterly sea breezes or plain winds dominate during the day, and westerly land breezes or mountain winds prevail at night under stable conditions. However, the combined influence of sea-land breezes and mountain-plain winds complicates the identification of a single dominant east-west-oriented wind structure and driving mechanism, warranting further analysis in subsequent sections.

Table 2 summarizes data from 18 representative meteorological stations, categorized into Valley, Coastal, Urban, and Rural groups, comparing key features of local winds: occurrence frequency, onset time, average wind direction, and speed. Valley and Sea stations recorded higher local wind frequencies than Urban and Rural stations. Urban proximity reduced local wind frequency by ~20 %, reflecting the spatial trends in diurnal and nocturnal wind speeds (O_{ws} & C_{ws}). Valley stations exhibited earlier diurnal wind onset (around 9:00 am) compared to Urban stations, while nocturnal winds in urban areas showed delays of 1-2 h, increasing with proximity to the city center.

Fig. 4 illustrates diurnal wind direction variations at four

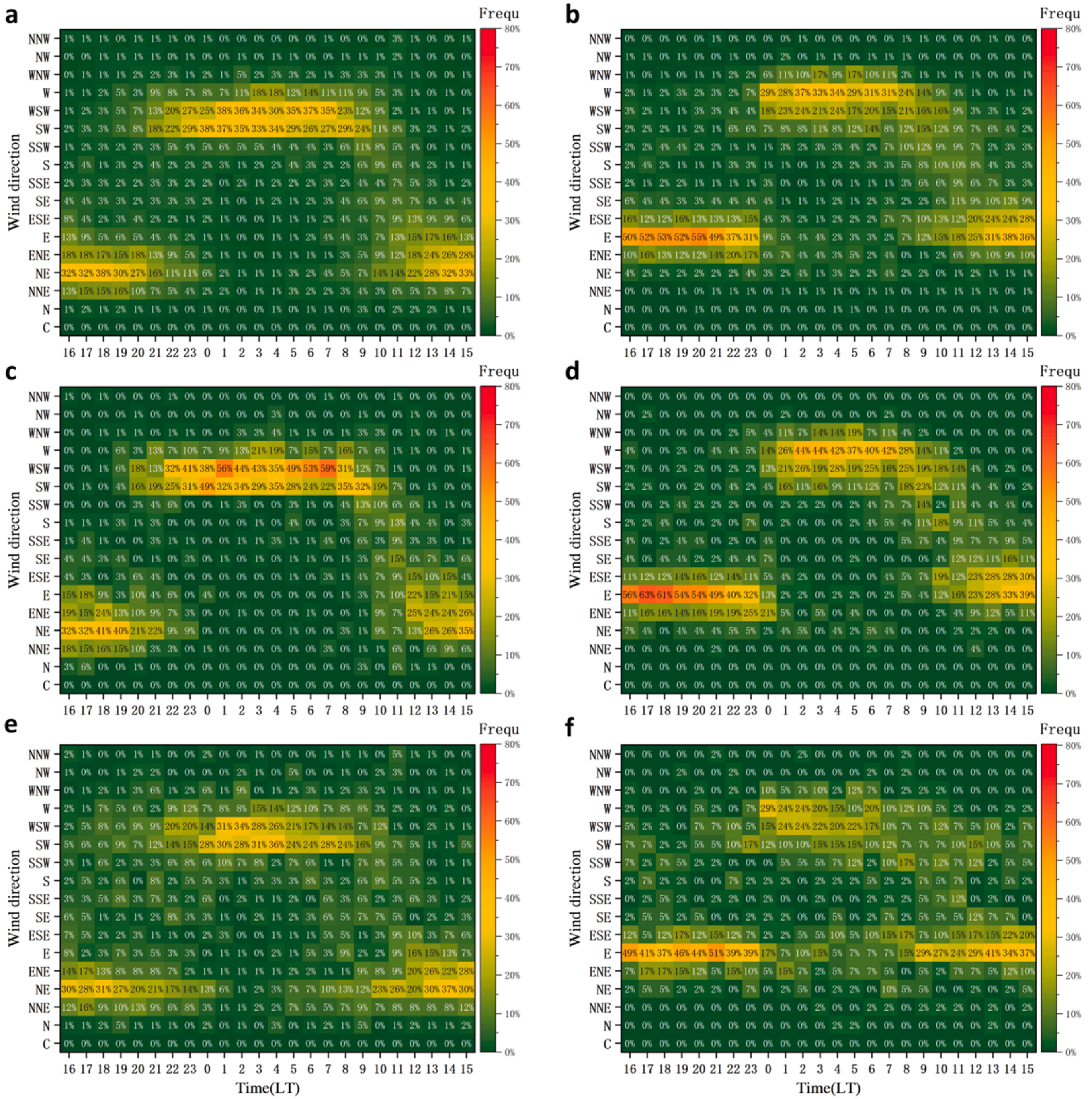

Fig. 7. Hourly occurrence probabilities of 16-directional winds throughout the day. Panels (a), (c), and (e) represent climatological conditions, strong UHI intensity events, and weak UHI intensity events at the meteorological station on the western side of the city (ID K1418), respectively. Panels (b), (d), and (f) show the same classifications for the meteorological station on the eastern side of the city (ID K1181). Locations of these four stations are indicated in Fig. 1a.

representative stations. Mountain-plain winds on the city's western side and sea–land breezes near Hangzhou Bay exhibit relatively consistent wind direction characteristics, with wind direction shifts around 8:00–9:00 am and 19:00–20:00 pm, supporting the interaction between these local circulations. Interestingly, sea–land breezes near the northern and southern bay (Fig.s 5c and 5d) exhibit anticlockwise and clockwise trajectories, diverging from typical Northern Hemisphere patterns (Shou et al., 2023). These anomalies may result from pressure gradient differences across the gulf, influenced by broader continental effects (Physick and Scott, 1977).

4.2. Diurnal Variations and transitions in Surface Wind Fields

Under stable atmospheric conditions, mountain-valley winds and sea-land breezes commonly induce diurnal variations in wind direction. While earlier studies suggested that these winds may act independently (Yu et al., 2021; Zhou, 1994), this study hypothesizes that both systems interact to influence the region. To test this, a cross-section along the dominant east-west wind axis (Fig. 1a) was analyzed using ten representative stations to examine wind direction transitions.

Fig. 6 illustrates the spatial variability of wind direction transitions along the transect. In the 'independent' scenario, wind systems such as mountain breezes and sea breezes evolve separately without mutual

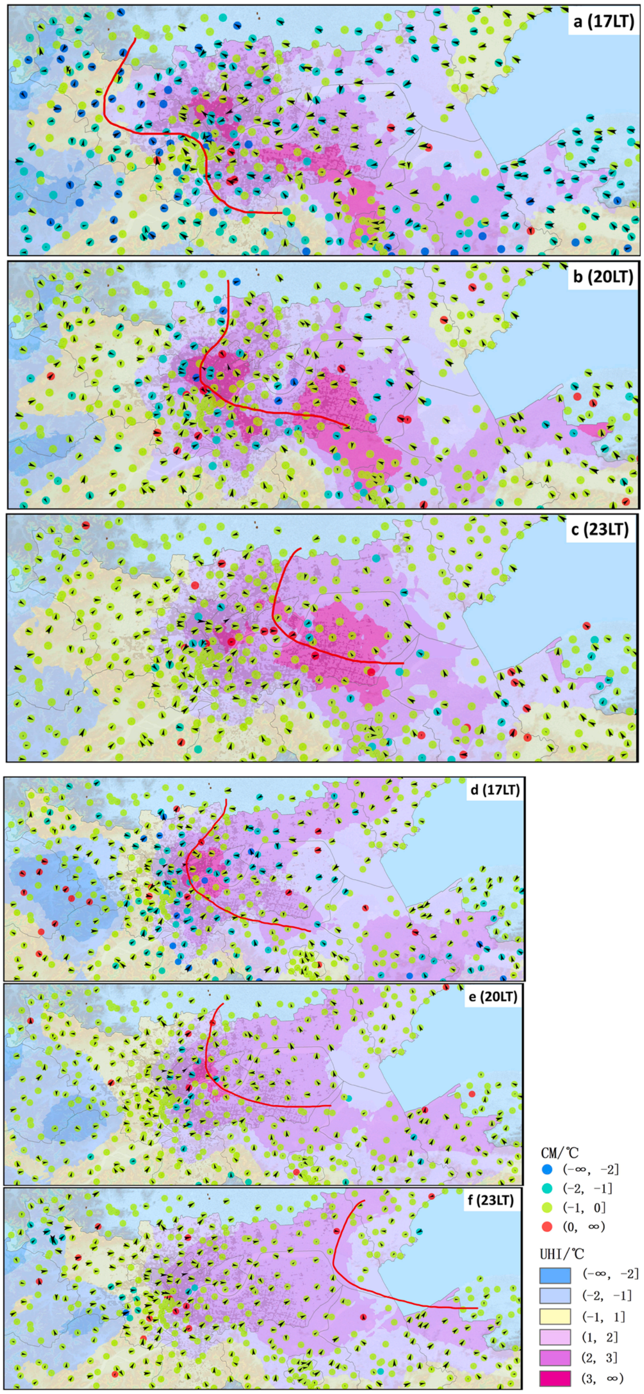

Fig. 8. Spatial distributions of 3-hourly surface wind fields, urban heat island (UHI) intensity, cooling magnitude (CM), and local circulation front positions for strong (a, b, c; July 24–25, 2017) and weak (e, f, g; June 1–2, 2018) UHI cases. CM represents the hourly cooling magnitude, while UHI denotes the urban heat island intensity index. Red curves mark the approximate locations of local circulation fronts inferred from the wind fields, and black arrows indicate wind direction and speed at meteorological stations.

interference—for example, mountain breezes would trigger sequential wind shifts from west to east. However, our observations (Fig. 6) show simultaneous wind reversals at both eastern (coastal) and western (mountainous) edges, while urban centers exhibit delayed transitions (green and red arrows). This pattern indicates that sea breezes and mountain winds interact, rather than operate independently. These wind patterns are further modulated by urban heat island (UHI) effects, which amplify or dampen local circulations depending on the time of day and prevailing atmospheric conditions.

Fig. 7 illustrates the modulation of local wind patterns by urban heat island (UHI) effects, with stable wind directions defined as probabilities exceeding 30 % over consecutive intervals. At the K1418 station (western city), strong UHI events (Fig. 7c) advance the stabilization of westerly winds to 20:00–21:00, approximately 1–2 h earlier than climatological conditions (Fig. 7a). This suggests UHI-induced winds enhance mountain and land breezes, facilitating the shift from easterly to westerly winds. Under weak UHI conditions (Fig. 7e), transitions occur later, at 21:00–22:00, resembling climatological patterns. Additionally, strong UHI increases the stability of westerly winds, with WSW and SW directions reaching nearly 50 % probability, while weak UHI produces more variable wind patterns. At the K1181 station (eastern city), weak UHI maintains a westerly wind transition around 23:00–00:00, consistent with climatological conditions, whereas strong UHI delays the transition past midnight and results in more dispersed nocturnal wind directions (Fig. 7d).

These findings highlight the complex interplay between urban heat island (UHI) circulations, mountain-plain winds, and sea-land breezes, as modulated by UHI intensity (Savijärvi et al., 2001). Strong UHI accelerates wind direction shifts in the western city while delaying transitions in the eastern city, reflecting the spatial variability of its impacts. Studies examining the simultaneous influence of mountain winds, sea-land breezes, and UHI circulations remain limited (Papanastasiou et al, 2010). Idealized WRF simulations have typically portrayed topography between the coast and the city as a barrier that inhibits sea-breeze penetration, thereby reducing cooling potential and intensifying urban heat accumulation (Du et al, 2024). In contrast, our findings identify a distinct wind regime shaped by a terrain configuration where the city is situated between mountains and the ocean. Under such conditions, UHI intensity modulates the phasing and coupling of local circulations. Notably, we show that mountain winds—often underappreciated—play a dominant role in nocturnal cooling and significantly improve urban ventilation. The combined influence of UHI effects, local topography, and coastal proximity underscores the intricate wind dynamics in Hangzhou, warranting further investigation to unravel these multifaceted interactions.

4.3. Local wind cases under different UHI intensities

This section examines the interaction between local wind dynamics and varying urban heat island (UHI) intensities, comparing two summer cases under similar stable atmospheric conditions with maximum hourly wind speeds below 6 m/s and the presence of mountain and sea breezes (Fig. 8).

Strong UHI Case (July 24–25, 2017): In this case, the UHI intensity peaked at 4.7°C and remained above 3.0°C for 24 h. At 17:00 on July 24, easterly sea/land breezes dominated the urban area, while westerly mountain winds had already reached the western and mountainous regions. By 18:00, mountain winds advanced into the western urban periphery but were obstructed by the intense heat island, halting further eastward penetration. It was not until 23:00 that mountain winds extended to the eastern outskirts, where they were again halted by another heat island center. By 02:00 on July 25, following the breakdown of the eastern heat island circulation, mountain/land winds reached Hangzhou Bay.

Weak UHI Case (June 1–2, 2018): Under weaker conditions, the UHI peaked at 2.6°C and remained above 2.0°C for only 5 h. Mountain winds reached the city's edge before 17:00 and faced minimal resistance from the dispersed and transient heat island zones. By 20:00, these winds crossed the urban core, merging with land breezes to reach Hangzhou Bay by 23:00.

The comparison between strong and weak UHI conditions highlights the pivotal role of UHI intensity in shaping local wind dynamics and cooling effects (Bastin et al., 2006; Shi et al., 2024). Strong UHIs act as

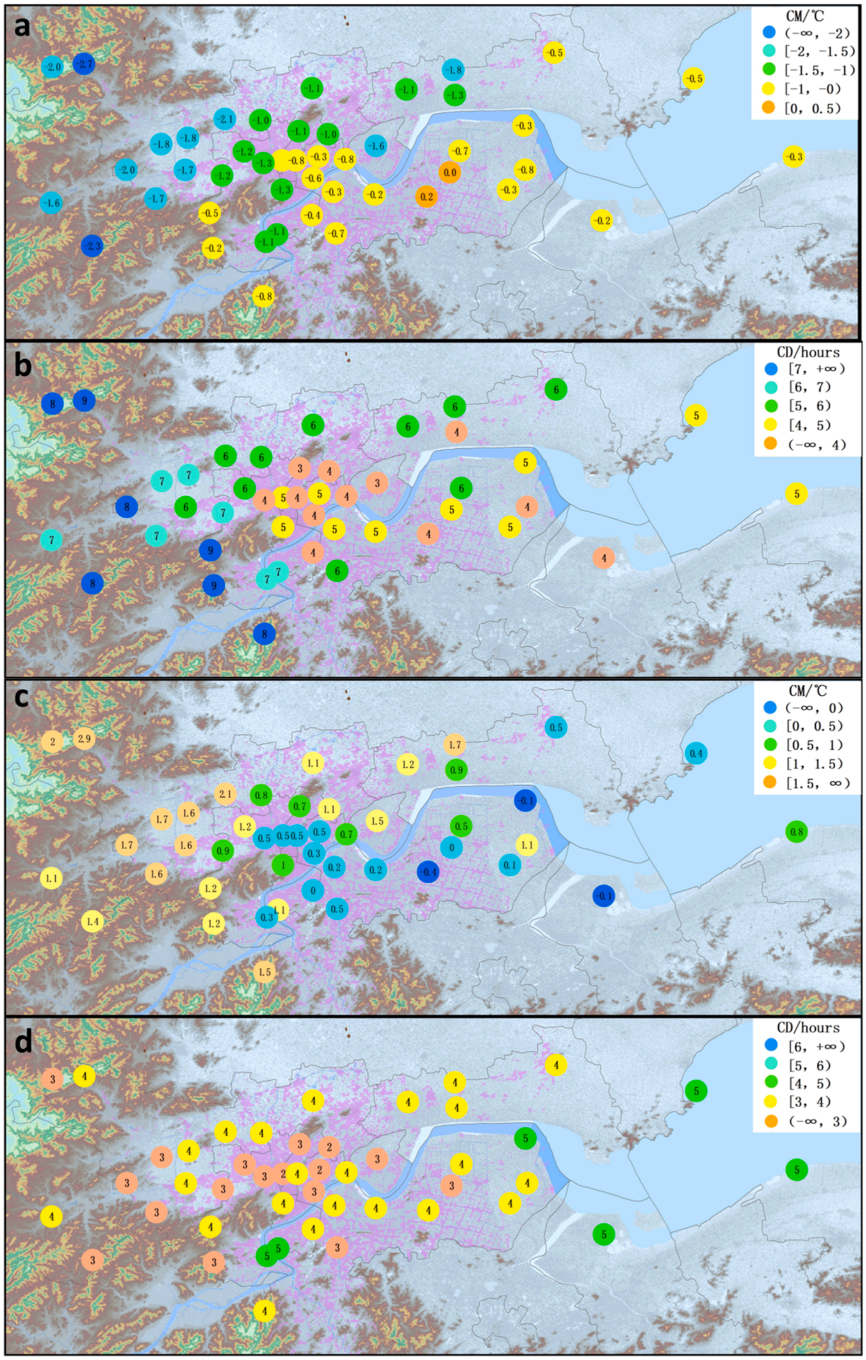

Fig. 9. Average hourly cooling magnitude (CM) and cumulative cooling duration (CD) at each climatic stations (CS) during nighttime and daytime, with day/night division based on sunrise and sunset times. Panels a and b show CM and CD during the night, while panels c and d show CM and CD during the day. Shaded areas represent elevation, with the purple region indicating the urban area, as in Fig. 1a.

barriers, delaying mountain wind progression and confining cooling effects to areas west of heat island centers. In contrast, weak UHIs enable smoother wind penetration, allowing earlier and broader cooling within urban areas, particularly evident after 20:00 (Fig. 8b, 8e). Mountain winds can lower temperatures by up to 6°C per hour at 17:00, effectively reducing intense UHI zones, though their cooling effect diminishes in stable, expansive heat islands. These findings underscore the need for cluster-based urban designs to fragment heat island zones and enhance local wind-driven cooling, mitigating heat stress in urban areas.

4.4. Cooling effects of local winds

4.4.1. Cooling effects on air temperatures

Mountain and sea-land breezes play critical roles in cooling urban environments and mitigating heat. This section evaluates their impacts during 41 high-temperature events (daily maximum temperature >35°C), with hourly cooling magnitude (CM) and cooling duration (CD) adjusted against a climatological baseline to isolate local wind effects.

Nocturnal Cooling: A distinct west-to-east cooling gradient emerges at night, with stations near the western mountains and urban periphery experiencing pronounced and sustained cooling (Fig. 9a, b). Baseline-adjusted hourly cooling exceeds 2°C on average, particularly between

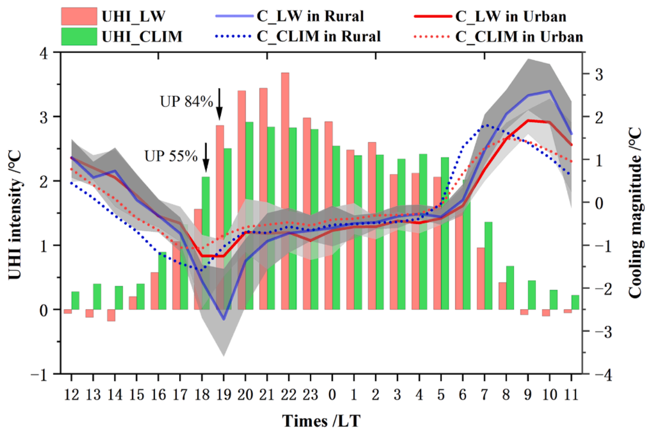

Fig. 10. Diurnal variations in UHI intensity and hourly cooling magnitude of air temperature under local winds and climatological conditions. Solid red and blue lines show CM diurnal variations for Urban and Rural stations under local winds, while dashed lines represent climatological conditions. Shaded areas indicate the 10th–90th percentile range. Red bars depict UHI under local winds, and green bars show UHI under climatological conditions.

Table 3
Fundamental characteristics of UHI and UCI intensity, as well as warming and cooling transitions, under mixed local wind conditions. The table includes key metrics such as onset time, peak time, and peak intensity for different meteorological station types: URB-S, SUB-S, VAL-S, and SEA-S.

Type	URB-S	RUR-S	VAL-S	SEA-S
Onset of UHI (LT)	—	17	18	All Day
Peak(°C) /Time(LT) of UHI	—	2.8 /02∼05	6.9 /01	3.8 /19
Onset of UCI	—	09	10	—
Peak(°C) /Time(LT) of UCI	—	-1.4 /12	-2.4/16	—
Onset of Heating (LT)	07	06	06	07
Peak(°C) /Time(LT) of warming	1.7 /09	2.9 /08	4.3/09	1.9 /10
Onset of Cooling(LT)	15	15	16	14
Peak(°C) /Time(LT) of Cooling	-1.1 /18	-1.7 /20	-4.3 /19	-1.8 /19

17:00 and 19:00, aligning with the onset and eastward penetration of mountain winds. Without baseline adjustments, cooling can surpass 10°C in specific cases. In contrast, stations near Hangzhou Bay exhibit limited cooling, with nocturnal CD only 60 % of that in mountainous areas. These results highlight the dominant role of westerly mountain winds as primary cooling drivers, though their effect diminishes as they progress eastward into urban cores.

Daytime Cooling: Daytime cooling effects are weaker overall. Unlike the nocturnal gradient, CD decreases from Hangzhou Bay toward the western mountains, with CM showing minor cooling near the bay but warming elsewhere (Fig. 9c, d). This indicates that daytime cooling is primarily driven by sea breezes, peaking between 14:00 and 17:00, with limited impact in urban cores. Events without baseline adjustment reveal isolated cases where sea breezes achieve cooling exceeding 5°C, underscoring their localized impact.

These findings demonstrate the spatial and temporal variability of local wind cooling effects. Nocturnal mountain winds provide substantial heat relief in western urban peripheries, while daytime sea breezes contribute localized cooling near coastal areas. Together, these breezes complement each other in regulating urban temperatures. These insights emphasize the importance of integrating local wind patterns into urban planning strategies.

4.4.2. Cooling effects on UHI intensity

Local winds, such as mountain and sea-land breezes, are known to cool surface temperatures effectively in the Hangzhou region. While numerical simulations suggest these winds mitigate urban heat island (UHI) intensity (Du et al., 2024; Yang et al., 2022; Zhou et al., 2020), observational data reveal more nuanced effects. As shown in Section 4.2.1, mountain breezes reduce the spatial extent of heat islands; however, their impact on overall UHI intensity does not always align with theoretical predictions.

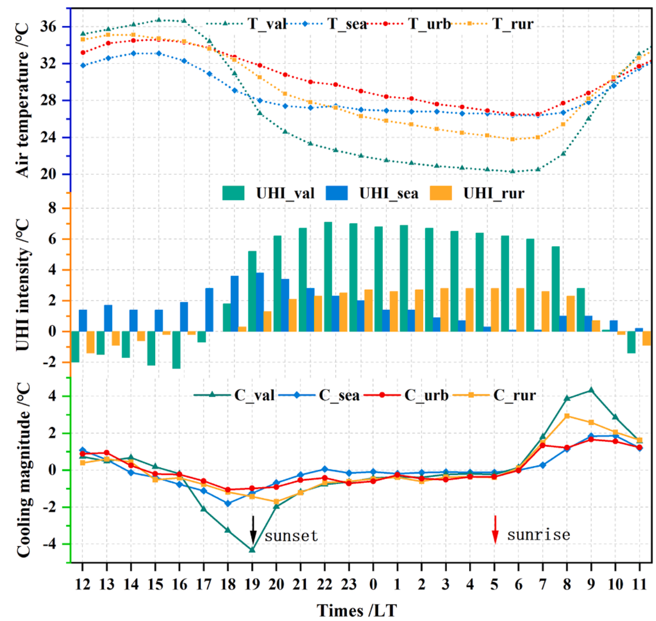

Fig. 11. Diurnal variations in UHI intensity, air temperature, and hourly cooling magnitude under local wind conditions. Dashed lines represent the air temperature variations of meteorological stations influenced by different local wind types, while solid lines show the hourly temperature changes for each station type. Bar charts display the UHI intensity (hourly temperature differences between different station types and the urban station). Different colors indicate different station types. Red and black arrows represent the sunrise and sunset times during summer (July–September) in Hangzhou, respectively. Locations of four type stations are indicated in Fig. 1a & 1c.

Fig. 10 highlights the differences in UHI behavior under climatological conditions compared to scenarios influenced by local winds. Under climatological conditions, Hangzhou exhibits a weak daytime heat island and a pronounced nighttime heat island. UHI intensity increases significantly during the evening transition period (17:00–18:00), rising by 55 % as heat accumulates in urban areas. When local winds are present, two distinct patterns emerge:

Under local wind influence, a weak “cool island” effect replaces the typical daytime heat island. Enhanced solar radiation accelerates warming at rural stations near mountains or bare land, which have lower heat capacity (Dewan et al., 2021), while urban areas, with higher heat capacity, warm more slowly. This reduces the urban-rural temperature contrast, creating an urban cooling anomaly (Dinda et al., 2022). In contrast, climatological conditions with weaker or diffuse radiation maintain a consistent urban-rural contrast, suppressing the ‘cool island’ effect.

During the 18:00–19:00 transition period, UHI intensity increases sharply by 84 % under local wind conditions, compared to a 55 % increase under climatological conditions. This surge corresponds to the onset of mountain breezes, which cool rural areas more significantly than urban zones. The enhanced rural cooling amplifies the temperature gradient between urban and rural stations, paradoxically intensifying the apparent UHI intensity. Rural stations experience marked cooling between 18:00–21:00, while urban temperatures remain relatively stable.

4.4.3. How local winds afffect UHI intensity

To examine how local wind types affect UHI intensity and optimize reference station selection, we analyzed three station types for rural

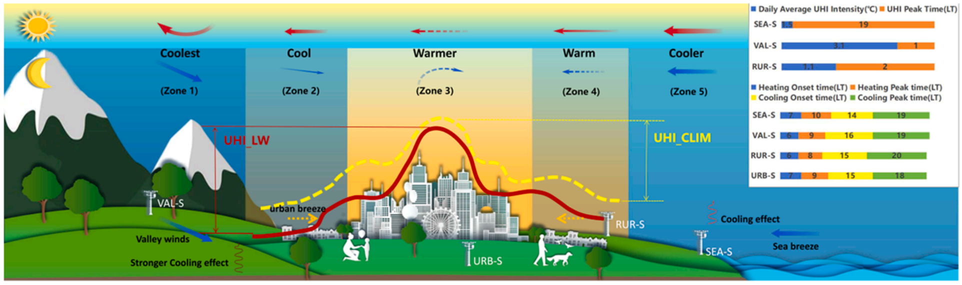

Fig. 12. Conceptual diagram illustrating the impact of local winds on urban wind structures and cooling effects. The diagram illustrates daytime (top, sun icon) and nighttime (bottom, moon icon) wind patterns, with line thickness indicating wind speed. The study area is divided into five zones: mountain (zone1), western rural (zone2), urban (zone3), eastern rural (zone4), and coastal (zone5). Yellow dashed (UHI_CLIM) and red solid (UHI_LW) lines represent suburban temperature profiles under climatological and local wind conditions, respectively. Local winds enhance cooling in rural zones, increasing urban–rural thermal contrast and potentially amplifying apparent UHI intensity. URB-S, SUB-S, VAL-S, and SEA-S refer to representative stations in urban, suburban, mountainous, and coastal areas.

station selection: SEA-S (K5519), VAL-S (K1044), SUB-S (K1210), and one fixed urban station URB-S (K1163) (Table 3 & Fig. 1a, 1c). While the location of SEA-S (K5519) is visible in Fig. 1a due to display range limitations, the positions of the other three stations are shown in Fig. 1c. Unlike Section 4.4.2, which contrasts climatological and local wind conditions, this analysis highlights diurnal UHI variations across diverse geographic environments under local wind scenarios (Fig. 11).

Fig. 11 and Table 3 demonstrate notable differences in the diurnal variation of UHI intensity among the three station types under local wind conditions. VAL-S stations exhibit the most pronounced variability, with peak UHI intensity reaching 6.9°C at 01:00 and a daytime cool island effect of -2.4°C at 16:00. These extremes highlight the strong influence of mountain winds on local temperature contrasts. SUB-S, located near urban peripheries, show trends similar to URB-S but with smaller hourly differences, likely due to slightly lower anthropogenic heat emissions while other environmental factors remain comparable (Ooi et al., 2017). This stability reinforces the reliability of URB-S measurements for UHI assessments, as they are less influenced by local wind effects or other external factors.

In contrast, SEA-S stations display distinct patterns, with peak UHI intensity occurring earlier in the evening (19:00), diverging from the midnight peaks at VAL-S and SUB-S. This difference is likely attributed to the high thermal inertia of seawater (Solcerova et al., 2018), which dampens temperature fluctuations and results in weaker overall UHI effects during the night. Particularly striking is the cooling effect at VAL-S during the onset of mountain breezes, with hourly cooling reaching 4.3°C at 19:00 (Fig. 11), coinciding with their eastward progression as seen in Fig. 7.

The influence of local winds on UHI intensity follows a clear hierarchy, with VAL-S exerting the greatest impact, followed by SEA-S and SUB-S. This variability underscores the potential for local winds to misrepresent UHI intensity, particularly by amplifying rural cooling and overstating urban-rural temperature contrasts (Cui et al., 2023; He et al., 2020). As shown in Fig. 11, compared to climatological conditions, local winds can significantly cool urban and surrounding areas but may paradoxically lead to an overestimation of UHI intensity.

Fig. 12 illustrates the diurnal mechanisms of local wind interactions in the Hangzhou Bay area. During the day, prevailing easterly sea breezes and plain winds weaken as they move inland due to surface friction and urban roughness, while upslope flows near the western mountains show a similar reduction approaching the city. At night, the interplay among mountain winds, sea-land breezes, and UHI-induced flows creates complex circulation patterns. Westerly mountain winds develop earlier, while sea breezes linger in coastal areas. In urban-suburban transition zones, these opposing flows converge, with UHI effects enhancing the urban-rural temperature gradient and modulating wind penetration. Friction and thermal contrasts further delay the eastward advance of mountain winds until late evening. Overall, while local winds cool suburban areas, they also intensify thermal contrasts, emphasizing the need to account for local circulation when assessing UHI intensity.

5. Conclusions

This study employed a standardized framework and high-resolution meteorological data to examine the interactions and cooling capacities among multiple local wind systems in Hangzhou, a region characterized by complex topography. The key findings are:

1. **Local Winds Identification and Interactions.** This study establishes a novel framework for detecting mixed local wind regimes by integrating multi-source meteorological observations with diurnal wind-phase analysis. In Hangzhou Bay's complex terrain, sea breezes, valley winds, and UHI circulations frequently occur (29-57 %), forming compound systems.. Using diurnal phase shifts, we quantified their synergistic interactions: daytime easterly breezes gradually transition to nocturnal westerly mountain winds. UHI intensity modulates these transitions-strong UHI delays mountain wind onset and weakens cooling, while weaker UHI facilitates continuous flow and urban ventilation. These findings reveal the dynamic coupling between multiple local circulations and urban thermal patterns.
2. **Cooling Effects of Local Winds**. We propose a novel approach to quantify cooling effects from local circulations. Results show strong nocturnal cooling from mountain winds, particularly in western areas, while sea breezes provide modest daytime relief near the coast. However, local winds can also heighten UHI effects by intensifying thermal contrasts, highlighting the nonlinear nature of wind–temperature interactions in urban settings.
3. **Reference Station Selection for UHI Assessment**. Local winds can significantly distort UHI intensity measurements. This study emphasizes the importance of carefully selecting reference stations to avoid misinterpretation from wind-driven temperature anomalies. Improved observational strategies are needed to separate the contributions of local circulations from broader climatic signals in UHI analyses.

While the study provides valuable insights, several limitations warrant further discussion:

1. Regional Specificity and General Implications. Hangzhou Bay's unique geography—bounded by mountains and the sea—shapes region-specific wind behaviors. Although the exact timing and intensity of wind shifts may not be universal, the underlying mechanisms governing multiscale wind interactions and their modulation of UHI are widely applicable to other complex terrains.
2. Observational–Modeling Synergy and Future Directions. While this study is grounded in high-density observations, it also reveals discrepancies with previous numerical results, underlining the need for

observational benchmarks. Numerical models (e.g., WRF) offer valuable tools to test terrain and land use sensitivities under controlled settings. Integrating observational and modeling approaches will refine our understanding of terrain–UHI–wind feedbacks and enhance the simulation of urban climates. Future studies should also explore the sensitivity of terrain parameters (e.g., mountain height and bay width) through numerical experiments to quantify their influence on local wind dynamics and urban thermal regulation.

3. Implications for Climate-Responsive Urban Planning. The findings highlight the potential of leveraging natural wind resources for urban cooling. Future research should incorporate local wind dynamics into planning strategies to optimize ventilation, reduce heat stress, and assess resilience under urban expansion and climate change. Understanding how local winds behave under extreme heat and altered landscapes will be key to designing future-ready, climate-resilient cities.

CRediT authorship contribution statement

Bu Yu: Writing – review & editing, Writing – original draft, Methodology, Data curation, Conceptualization. **Zhiwen Luo:** Supervision, Methodology, Conceptualization. **Feng Chen:** Project administration, Investigation, Funding acquisition, Data curation. **Peng Xie:** Software, Data curation. **Shiguang Miao:** Supervision, Investigation, Formal analysis. **Yige Zhong:** Visualization.

Declaration of competing interest

The authors declare the following financial interests/personal relationships which may be considered as potential competing interests:

Feng Chen reports financial support was provided by National Science Foundation of China. If there are other authors, they declare that they have no known competing financial interests or personal relationships that could have appeared to influence the work reported in this paper.

Acknowledgments

This study was supported by the National Science Foundation of China (42475038), Key Laboratory of Urban Meteorology, China Meteorological Administration(LUM-2024-18), and Hangzhou Urban Meteorology Joint Laboratory Research Projects (SYSYB202406). BY would like to acknowledge the China Scholarship Council funding (202305330011) to support his academic visit at Cardiff University, where this research has been conducted.

Data availability

Data will be made available on request.

References

Alomar-Garau, G., & Grimalt-Gelabert, M. (2022). Impacts of coastal breezes on the environment and Human life: The case of Mallorca (Western Mediterranean). *Coasts, 2*(1), 17–35. https://doi.org/10.3390/coasts2010002

Arrillaga, J. A., Jiménez, P., Vilà-Guerau De Arellano, J., Jiménez, M. A., Román-Cascón, C., Sastre, M., & Yagüe, C. (2020). Analyzing the synoptic-, meso- and local-scale involved in sea breeze formation and frontal characteristics. *Journal of Geophysical Research: Atmospheres, 125*(4), Article e2019JD031302. https://doi.org/10.1029/2019JD031302

Azorin-Molina, C., & Chen, D. (2009). A climatological study of the influence of synoptic-scale flows on sea breeze evolution in the Bay of Alicante (Spain). *Theoretical and Applied Climatology, 96*(3–4), 249–260. https://doi.org/10.1007/s00704-008-0028-2

Barlow, J. F. (2014). Progress in observing and modelling the urban boundary layer. *Urban Climate, 10*, 216–240. https://doi.org/10.1016/j.uclim.2014.03.011

Bastin, S., & Drobinski, P. (2006). Sea-breeze-induced mass transport over complex terrain in south-eastern France: A case-study. *Quarterly Journal of the Royal Meteorological Society, 132*(615), 405–423. https://doi.org/10.1256/qj.04.111

Cheng, F., Wang, Y., Huang, M., Lin, P., Lin, C., Lin, P., Wang, S., & Tsuang, B. (2022). Boundary layer characteristics over complex terrain in Central Taiwan: Observations and numerical modeling. *Journal of Geophysical Research: Atmospheres, 127*(2), Article e2021JD035726. https://doi.org/10.1029/2021JD035726

Cui, F., Hamdi, R., Kuang, W., Yang, T., He, H., Termonia, P., & De Maeyer, P. (2023). Interactions between the summer urban heat islands and heat waves in Beijing during 2000–2018. *Atmospheric Research, 291*, Article 106813. https://doi.org/10.1016/j.atmosres.2023.106813

Dai, A., Trenberth, K. E., & Karl, T. R. (1999). Effects of clouds, soil moisture, precipitation, and water vapor on diurnal temperature range. *Journal of Climate, 12*(8), 2451–2473. https://doi.org/10.1175/1520-0442(1999)012<2451:EOCSMP>2.0.CO;2

Dewan, A., Kiselev, G., Botje, D., Mahmud, G. I., Bhuian, Md. H., & Hassan, Q. K. (2021). Surface urban heat island intensity in five major cities of Bangladesh: Patterns, drivers and trends. *Sustainable Cities and Society, 71*, Article 102926. https://doi.org/10.1016/j.scs.2021.102926

Dinda, A., & Chatterjee, S. (2022). Assessing the local- impacts of heat advection on urban heat islands in Kolkata Metropolitan Area. *Urban Climate, 42*, Article 101139. https://doi.org/10.1016/j.uclim.2022.101139

Du, R., Liu, C. H., Li, X., & Lin, C. Y. (2024). Interaction among local flows, UHI, coastal winds, and complex terrain: Effect on urban-scale temperature and building energy consumption during heatwaves. *Energy and Buildings, 303*, Article 113763. https://doi.org/10.1016/j.enbuild.2023.113763

Dupuis, D. J., & Trapin, L. (2020). Structural change to the persistence of the urban heat island. *Environmental Research Letters, 15*(10), Article 104076. https://doi.org/10.1088/1748-9326/abb158

Falasca, S., Zinzi, M., Siani, A. M., Curci, G., Ding, L., & Santamouris, M. (2024). Investigating the effects of the greenery increase on air temperature, ventilation and cooling energy demand in Melbourne with the weather research and forecasting model and local climate zones. *Science of The Total Environment, 953*, Article 176016. https://doi.org/10.1016/j.scitotenv.2024.176016

Freitas, E. D., Rozoff, C. M., Cotton, W. R., & Dias, P. L. S. (2007). Interactions of an urban heat island and sea-breeze circulations during winter over the metropolitan area of São Paulo, Brazil. *Boundary-Layer Meteorology, 122*(1), 43–65. https://doi.org/10.1007/s10546-006-9091-3

Gray, L. J., Beer, J., Geller, M., Haigh, J. D., Lockwood, M., Matthes, K., Cubasch, U., Fleitmann, D., Harrison, G., Hood, L., Luterbacher, J., Meehl, G. A., Shindell, D., Van Geel, B., & White, W. (2010). Solar influences on climate. *Reviews of Geophysics, 48*(4), RG4001. https://doi.org/10.1029/2009RG000282

Han, Z. S., Liu, H. N., Yu, B., & Wang, X. Y. (2023). The effects of coastal local circulations and their interactions on ozone pollution in the Hangzhou metropolitan area. *Urban Climate, 48*, 101417. https://doi.org/10.1016/j.uclim.2023.101417

He, J., Chen, D., Gu, Y., Jia, H., Zhong, K., & Kang, Y. (2022). *Evaluation of planetary boundary layer schemes in WRF model for simulating sea-land breeze in Shanghai, 278*. China: Atmospheric Research, Article 106337. https://doi.org/10.1016/j.atmosres.2022.106337

He, X., Wang, J., Feng, J., Yan, Z., Miao, S., Zhang, Y., & Xia, J. (2020). Observational and modeling study of interactions between urban heat Island and heatwave in Beijing. *Journal of Cleaner Production, 247*, Article 119169. https://doi.org/10.1016/j.jclepro.2019.119169

Hirsch, A. L., Evans, J. P., Thomas, C., Conroy, B., Hart, M. A., Lipson, M., & Ertler, W. (2021). Resolving the influence of local flows on urban heat amplification during heatwaves. *Environmental Research Letters, 16*(6), Article 064066. https://doi.org/10.1088/1748-9326/ac0377

Junnaedhi, I. D. G. A., Inagaki, A., Ferdiansyah, M. R., & Kanda, M. (2023). Seasonal sea breeze variation analysis based on multi-year near-surface observations in Jakarta, Indonesia. *International Journal of Climatology, 43*(11), 5177–5195. https://doi.org/10.1002/joc.8139

Keeler, J. M., & Kristovich, D. A. R. (2012). Observations of urban heat island influence on Lake-Breeze Frontal movement. *Journal of Applied Meteorology and Climatology, 51*(4), 702–710. https://doi.org/10.1175/JAMC-D-11-0166.1

Kwok, Y. T., De Munck, C., Lau, K. K.-L., & Ng, E. (2022). To what extent can urban ventilation features cool a compact built-up environment during a prolonged heatwave? A mesoscale numerical modelling study for Hong Kong. *Sustainable Cities and Society, 77*, 103541. https://doi.org/10.1016/j.scs.2021.103541

Leckebusch, G., Koffi, B., Ulbrich, U., Pinto, J., Spangehl, T., & Zacharias, S. (2006). Analysis of frequency and intensity of European winter storm events from a multi-model perspective, at synoptic and regional scales. *Climate Research, 31*, 59–74. https://doi.org/10.3354/cr031059

Leo, L. S., Fernando, H. J. S., & Di Sabatino, S. (2015). Near-surface flow in complex terrain with coastal and urban influence. *Environmental Fluid Mechanics, 15*(2), 349–372. https://doi.org/10.1007/s10652-013-9327-y

Liu, X., Ming, Y., Liu, Y., Yue, W., & Han, G. (2022). Influences of landform and urban form factors on urban heat island: Comparative case study between Chengdu and Chongqing. *Science of The Total Environment, 820*, Article 153395. https://doi.org/10.1016/j.scitotenv.2022.153395

Lussana, C., Uboldi, F., & Salvati, M. R. (2010). A spatial consistency test for surface observations from mesoscale meteorological networks: Spatial consistency test for mesoscale networks. *Quarterly Journal of the Royal Meteorological Society, 136*(649), 1075–1088. https://doi.org/10.1002/qj.622

McGarity, A. E., & Gorski, A. I. (1984). Passive generation and storage of winter ice for summer cooling applications. *Energy Developments: New Forms, Renewables, Conservation* (pp. 245–250). Elsevier. https://doi.org/10.1016/B978-0-08-025407-4.50050-8

Merlone, A., Beges, G., Bottacin, A., Brunet, M., Gilabert, A., Groselj, D., Harper, A., Hechler, P., Ivanov, M., Musacchio, C., Trewin, B., & Wright, W. (2024).

Climatological reference stations: Definitions and requirements. *International Journal of Climatology, 44*(5), 1710–1724. https://doi.org/10.1002/joc.8406

Morris, C. J. G., Simmonds, I., & Plummer, N. (2001). Quantification of the influences of wind and cloud on the nocturnal urban heat island of a large City. *Journal of Applied Meteorology, 40*(2), 169–182. https://doi.org/10.1175/1520-0450(2001)040<0169:QOTIOW>2.0.CO;2

Ng, E., & Ren, C. (2015). *The urban climatic map: A methodology for sustainable urban planning*. Routledge. https://doi.org/10.4324/9781315717616

Ooi, M. C. G., Chan, A., Subramaniam, K., Morris, K. I., & Oozeer, M. Y. (2017). Interaction of urban heating and local winds during the calm intermonsoon seasons in the tropics. *Journal of Geophysical Research: Atmospheres*, (21), 122. https://doi.org/10.1002/2017JD026690

Papanastasiou, D. K., Melas, D., & Lissaridis, I. (2010). Study of wind field under sea breeze conditions; an application of WRF model. *Atmospheric Research, 98*(1), 102–117. https://doi.org/10.1016/j.atmosres.2010.06.005

Physick, W. L., & Byron-Scott, R. A. D. (1977). Observations of the sea breeze in the vicinity of a gulf. *Weather, 32*(10), 373–381. https://doi.org/10.1002/j.1477-8696.1977.tb04481.x

Prtenjak, M. T., & Grisogono, B. (2007). Sea/land breeze climatological characteristics along the northern Croatian Adriatic coast. *Theoretical and Applied Climatology, 90* (3–4), 201–215. https://doi.org/10.1007/s00704-006-0286-9

Ribeiro, F. N. D., Oliveira, A. P.de, Soares, J., Miranda, R. M.de, Barlage, M., & Chen, F. (2018). Effect of sea breeze propagation on the urban boundary layer of the metropolitan region of Sao Paulo, Brazil. *Atmospheric Research, 214*, 174–188. https://doi.org/10.1016/j.atmosres.2018.07.015

Savijärvi, H., & Liya, J. (2001). Local winds in a valley city. *Boundary-Layer Meteorology, 100*(2), 301–319. https://doi.org/10.1023/A:1019215031007

Shang, M., Cao, L., Guo, J., Guo, Z., Liu, L., & Zhong, S. (2024). Influence of pure sea breeze on urban heat island in Tianjin, China: A perspective from multiple meteorological observations. *Atmospheric Research, 304*, Article 107408. https://doi.org/10.1016/j.atmosres.2024.107408

Shi, T., Yang, Y., Qi, P., & Lolli, S. (2024). Diurnal variation in an amplified canopy urban heat island during heat wave periods in the megacity of Beijing: Roles of mountain–valley breeze and urban morphology. *Atmospheric Chemistry and Physics, 24*(22), 12807–12822. https://doi.org/10.5194/acp-24-12807-2024

Shou, S., Li, S., Shou, Y., & Yao, X. (2023). *An introduction to mesoscale meteorology*. Springer Nature Singapore. https://doi.org/10.1007/978-981-19-8606-2

Solcerova, A. (2018). *Water as a coolant of cities*. [Delft University of Technology]. https://doi.org/10.4233/UUID:CE45B39C-4A28-46A5-A90F-FAB989B132CE

Stewart, I. D., & Oke, T. R. (2012). Local climate zones for urban temperature studies. *Bulletin of the American Meteorological Society, 93*(12), 1879–1900. https://doi.org/10.1175/BAMS-D-11-00019.1

Wang, Haijun., Yang, Zhibiao., Yang, Daicai., & Gong, Xianchuang (2007). The method and application of automatic quality control for real time data from automatic weather stations. *Meteorological Monthly, 33*(10), 102–109. https://doi.org/10.7519/j.issn.1000-0526.2007.10.015. in Chinese.

Yang, J., Xin, J., Zhang, Y., Xiao, X., & Xia, J. C. (2022). Contributions of sea–land breeze and local climate zones to daytime and nighttime heat island intensity. *Npj Urban Sustainability, 2*(1), 12. https://doi.org/10.1038/s42949-022-00055-z

Yu, B., Zhu, B., Miao, S., Kang, H., He, X., Liu, H., Liang, Z., & Chen, F. (2021). Observational signal of the interaction between mountain–Plain wind and urban breeze under weak synoptic systems. *Journal of Geophysical Research: Atmospheres, 126*(8), Article e2020JD032809. https://doi.org/10.1029/2020JD032809

Zardi, D., & Whiteman, C. D. (2013). Diurnal mountain wind systems(M)//Mountain weather research and forecasting. *Springer Netherlands*, 35–119. https://doi.org/10.1007/978-94-007-4098-3-2

Zheng, Z., Lin, X., Chen, L., Yan, C., & Sun, T. (2024). *Effects of urbanization and topography on thermal comfort during a heat wave event: A case study of Fuzhou, 102*. China: Sustainable Cities and Society, Article 105233. https://doi.org/10.1016/j.scs.2024.105233

Zhou, J., Yang, K., Crow, W. T., Dong, J., Zhao, L., Feng, H., Zou, M., Lu, H., Tang, R., & Jiang, Y. (2023). Potential of remote sensing surface temperature- and evapotranspiration-based land-atmosphere coupling metrics for land surface model calibration. *Remote Sensing of Environment, 291*, Article 113557. https://doi.org/10.1016/j.rse.2023.113557

Zhou, Q. H. (1994). Some characteristics of sea-land breeze circulation over the coast of Hangzhou Bay. *Journal of Marine Sciences, 12*(3), 12–20. in Chinese https://d.wanfangdata.com.cn/periodical/QK199400033809.

Zhou, W., Yu, Y., Zhang, S., Xu, J., & Wu, T. (2025). Methods for quantifying the cooling effect of urban green spaces using remote sensing: A comparative study. *Landscape and Urban Planning, 256*, Article 105289. https://doi.org/10.1016/j.landurbplan.2024.105289

Zhou, X., Okaze, T., Ren, C., Cai, M., Ishida, Y., Watanabe, H., & Mochida, A. (2020). Evaluation of urban heat islands using local climate zones and the influence of sea-land breeze. *Sustainable Cities and Society, 55*, Article 102060. https://doi.org/10.1016/j.scs.2020.102060